

Hadron-proton elastic scattering at 50, 100, and 200 GeV/c momentum*

C. W. Akerlof, R. Kotthaus,[†] R. L. Loveless,[‡] and D. I. Meyer
Physics Department, University of Michigan, Ann Arbor, Michigan 48104

I. Ambats, W. T. Meyer,[§] and C. E. W. Ward
Argonne National Laboratory, Argonne, Illinois 60439

D. P. Eartly, R. A. Lundy, S. M. Pruss, and D. D. Yovanovitch
Fermi National Accelerator Laboratory, Batavia, Illinois 60510

D. R. Rust
Physics Department, University of Indiana, Bloomington, Indiana 47401

(Received 26 April 1976)

Elastic scattering of hadrons on protons has been measured at momenta of 50, 100, and 200 GeV/c. The meson-proton scattering is found to be independent of momentum and meson type for $-t > 0.8$ (GeV/c)². The momentum dependence of the pp dip at $-t = 1.4$ (GeV/c)² was investigated. Slope parameters are given.

INTRODUCTION

Elastic scattering is one of the most important measurements to be made whenever new energy regions become accessible. For a geometric model it provides information, through diffractive shadow scattering, on the size and opacity of the interaction region, and from the Regge point of view it gives information on the properties of the elusive Pomeron.

We have performed an experiment at Fermilab to measure the differential elastic-scattering cross section in the laboratory momentum range from 50 to 200 GeV/c. All of the long-lived hadrons π^{\pm} , K^{\pm} , p , and \bar{p} were used as projectiles to bombard hydrogen. The four-momentum-transfer range covered was $0.07 < -t < 1.6$ (GeV/c)². Proton-proton collisions were studied to a somewhat higher value of $-t$ to encompass the dip at $-t = 1.4$ (GeV/c)² which has been seen in data from the CERN ISR. Since this was one of the first experiments to explore the above range of parameters it was designed both to give accurate data in the small- t region and to explore the larger- t region.

At lower energies a useful compendium on elastic scattering is available.¹ The Serpukhov² results in the region just below 50 GeV/c serve as a comparison for our data. Above 200 GeV/c data³ from the ISR provide information on pp scattering. In addition, another experiment has been reported which overlaps the present one in the small- t region.⁴ The results to be presented here have been published in preliminary form.⁵

A major problem in designing the experiment was that the cross sections for elastic scattering change by over four decades in the t range of the experiment. If one chooses to collect data in

several consecutive t slices the relative normalization between the slices becomes a crucial parameter in the t distribution. Distorting the geometry severely to emphasize the high- t region also can result in experimental uncertainties. We chose to accept the entire t distribution at one time with almost constant azimuthal acceptance resulting in a large quantity of low- t data with which to measure slopes and shapes of cross sections. The large- t data are then of statistically lower quality.

The kinematics of forward elastic scattering at high energies is such that the recoiling-proton angle and energy are essentially independent of incoming momentum and particle type. Accordingly we use the recoil proton to determine the solid-angle acceptance since this minimizes systematic variations between energies and particle types. It is also the most natural way of instrumenting to give a constant azimuthal acceptance.

The background of inelastic channels must be discriminated against. At small t values the elastic cross section is much larger than any competing process. At the larger t values competing reactions are an important source of background. [In fact, $N^*(1688)$ production is larger than elastic pp scattering over part of the t range.] In designing the experiment it became clear that at least three constraints were needed to separate elastic events at large t . For one constraint we chose coplanarity defined as the angle of the beam relative to a plane determined by the recoil and forward particles. The other two constraints were the laboratory opening angle between the forward and recoil particles, and the missing mass of the recoil as measured by the momentum of the for-

ward-scattered particle and the beam. To use these constraints accurate angular measurements of the outgoing particles and the beam were necessary.

APPARATUS AND DATA ANALYSIS

The experiment was carried out in the M1A beam in the meson laboratory at Fermilab. A description of the beam intensity and fractional composition of various particles has been published.⁶ In order to define the angle of the beam sufficiently well to make use of the coplanarity and opening-angle constraints two scintillation-counter hodoscopes were built. One of these hodoscopes, immediately in front of the hydrogen target, had a position resolution of ± 0.75 mm and was made of 10 horizontal and 10 vertical overlapping counters. It served both to determine the transverse position of the beam particle at the target and as one element in measuring the beam angle. The second hodoscope, located 30 m upstream, was of similar construction but had half the position resolution of the first. These two hodoscopes determined angles to ± 0.08 mrad. Approximately 20% of the beam particles were counted in more than one element in at least one of the hodoscopes, probably because of δ rays and small-angle hadron showers in Čerenkov-counter mirrors and end windows. These events were rejected at the beginning of the analysis.

Particle identification was done by means of three Čerenkov counters in the beam. One of these was a threshold counter which was used largely to provide auxiliary separation for protons when they were the dominant beam component. The other two counters were of a semidifferential type which has been described in detail elsewhere.⁷ They operate by detecting particles in two categories defined by Čerenkov angles greater and less than a predetermined value. Pressure curves showed that the contamination of one particle type by another was negligible except for K^- at 200 GeV/c. The small fraction of K^- and difficulty of separation at 200 GeV/c resulted in a contamina-

tion of π^- 's which could be as large as 5%.

A drawing of the apparatus is shown in Fig. 1. In addition to the Čerenkov counters and hodoscopes a beam particle had to pass a veto counter with a 2.5-cm-diameter hole just upstream from the 30-cm-long hydrogen target. An event was defined by an acceptable beam particle plus a particle in both the forward and recoil arms of the spectrometer. To further limit spark-chamber triggers on events with more than one forward particle a veto counter behind two radiation lengths of Pb was placed 2.5 m downstream from the target. A hole in this counter was shaped to allow the forward particle from all elastic events to pass through. The combined trigger requirement resulted in approximately 40% of the triggers being reconstructed as elastic events.

Since the analysis required knowledge of the recoil-proton direction the lower limit on the four-momentum transfer was determined by the range of the recoil in the hydrogen target and the spark chambers. Because the very-low-momentum recoil protons are severely multiple-scattered, the acceptance criteria in coplanarity and opening angle were broadened considerably at low $-t$ so that these events were not lost. Fortunately the elastic cross section is very large in this t region, so the background was negligible even with the less stringent constraints. We have chosen $-t = 0.07$ (GeV/c)² as the lowest four-momentum at which we had full acceptance of recoils.

As stated above, the azimuthal acceptance was determined by the geometry of the recoil chambers. It is shown plotted vs $-t$ in Fig. 2. For 50 GeV/c beam momentum the upper limit on $-t$ was determined by the horizontal acceptance of the downstream analyzing magnets as illustrated in Fig. 2. For 100 GeV/c and 200 GeV/c the large $-t$ acceptance went beyond where the cross-section size fell below the sensitivity of the experiment.

The momentum resolution both of the beam and of the forward spectrometer was $\pm 0.5\%$. Folding in alignment systematics, etc., the overall momentum uncertainty between the beam and the

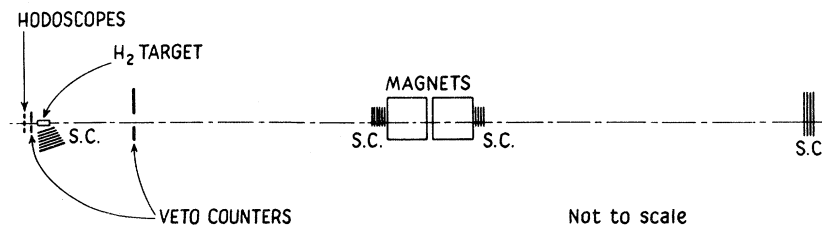


FIG. 1. Apparatus downstream from target. Čerenkov counters and upstream hodoscope are not shown.

forward-scattered particle gave a σ of approximately $\pm 1\%$. This was consistent with measurements made in the spectrometer on unscattered beam particles. The downstream analyzing magnets were set to bend 0.010 rad at 200 GeV/c and 0.020 rad at 50 and 100 GeV/c.

The accuracy of measurements on the opening angle between the recoil and forward particles is determined largely by the accuracy of the angular measurement on the recoil. A typical curve is shown in Fig. 3 for the difference between the measured and the expected elastic scattering opening angle. This gives a full width at half-maximum of 0.8 mrad excluding events of low $-t$ for which multiple scattering of the recoil is large. A typical coplanarity plot for the same $-t$ range is also shown in Fig. 3.

Angular-independent corrections to the data come from absorption in material in the forward and recoil arms, multiple hits and inefficiencies in the hodoscope, decays in flight, and μ and e contamination in the beam. All of these except for the hodoscope correction were less than a few percent and could be made in a standard way. The hodoscope correction was 20% as mentioned previously but was easily measured to high accuracy. The combined error on all these corrections was estimated to be around 1%. Several target-empty runs were made which yielded 0.1% as many events as with the target full. This small value is due to the requirement that the incoming track and the two outgoing tracks reconstruct to a point in the target.

The largest error in the absolute normalization was the uncertainty in the efficiency for reconstructing events from the spark-chamber data, particularly in the forward arm. The spark chambers in front of the magnet often recorded a large number of tracks from an obviously inelastic event, and sometimes it was impossible to tell if an elastic event was also buried in the debris. The seriousness of the problem varied greatly with

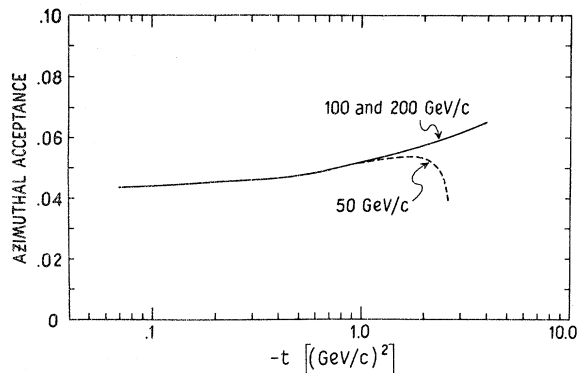


FIG. 2. Azimuthal acceptance as a function of t .

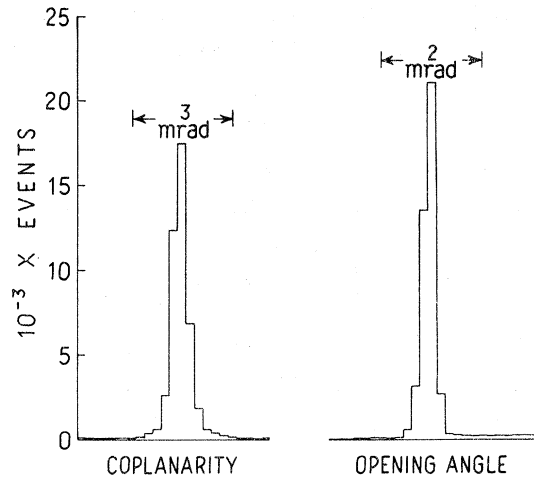


FIG. 3. Typical opening-angle (measured - expected) and coplanarity distributions after the cut on missing mass.

beam intensity and structure. It is largely because of this uncertainty that a $\pm 7\%$ error is quoted on the absolute normalization.

There were two t -dependent corrections which were made. One was the azimuthal acceptance which is shown in Fig. 2. A simple Monte Carlo calculation involving the parameters of the system, in particular the geometry of the beam and the recoil arm, determined this acceptance to high accuracy. The other correction was due to background from inelastic events and was determined by studying the coplanarity, opening-angle, and missing-mass distributions. Because of the three constraints, the background was not large except at high t . A typical background correction as a function of t is shown in Fig. 4.

The pp data for high $-t$ require separate consideration because the data-taking conditions dif-

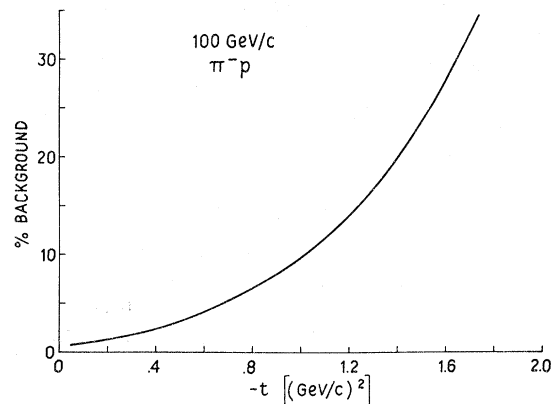


FIG. 4. Percent of events subtracted as background as a function of t for π^-p at 100 GeV/c.

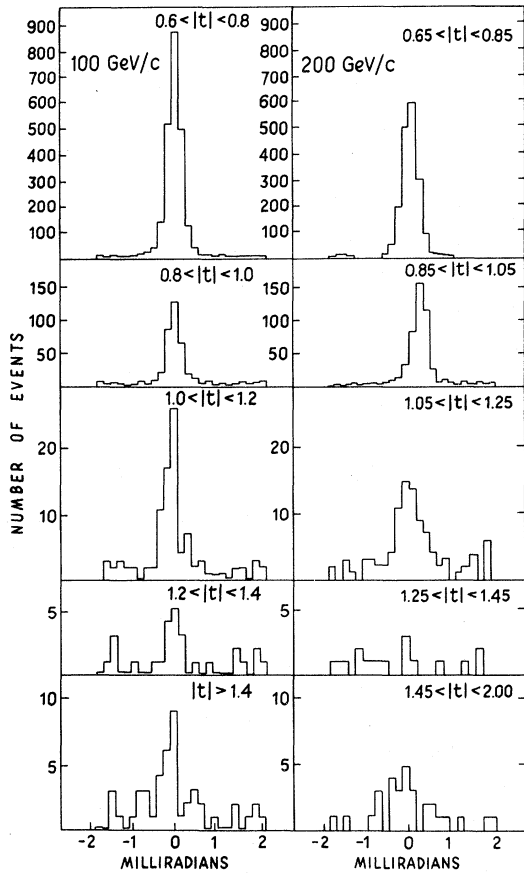


FIG. 5. Difference in measured and expected opening angle for large- $|t|$ 100- and 200-GeV/c pp interactions after missing-mass cut.

ferred from those of the rest of the experiment. These data were taken at high beam rates with the forward spark chambers moved so that the events at very low $-t$ did not go through them. The data were normalized relative to the small-angle data in the overlap region $0.6 < -t < 1.0$ GeV/c. A second difference was that because of the small cross sections beyond $-t = 1.0$ (GeV/c)² the background subtraction became a sizeable portion of the signal. The background encountered for the coplanarity and opening-angle distributions is shown in Figs. 5 and 6.

RESULTS

In the region of low $-t$ it is of interest to compare the particle and antiparticle cross sections. For π mesons isospin relates the amplitude of the elastic and charge-exchange cross sections through the equation

$$A(\pi^-p \rightarrow \pi^-p) - A(\pi^+p \rightarrow \pi^+p) = -\sqrt{2}A(\pi^-p \rightarrow \pi^0n).$$

Since the charge-exchange cross section⁸ falls

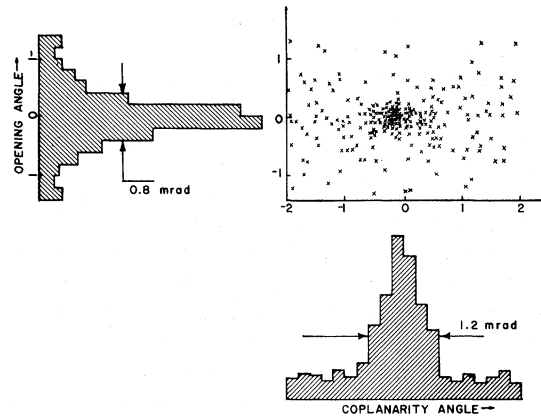


FIG. 6. Scatter plot of coplanarity and opening angle for 200-GeV/c pp scattering from $-t > 1.0$ (GeV/c)² after missing-mass cuts.

approximately as $1/s$ the two elastic cross sections should approach each other regardless of the phases of the amplitudes. The extent to which this has occurred at 200 GeV/c is illustrated in Fig. 7, where the data for the two reactions are indistinguishable. This is consistent with the size of the charge-exchange cross section and the vanishing of the Regge ρ -exchange contribution with

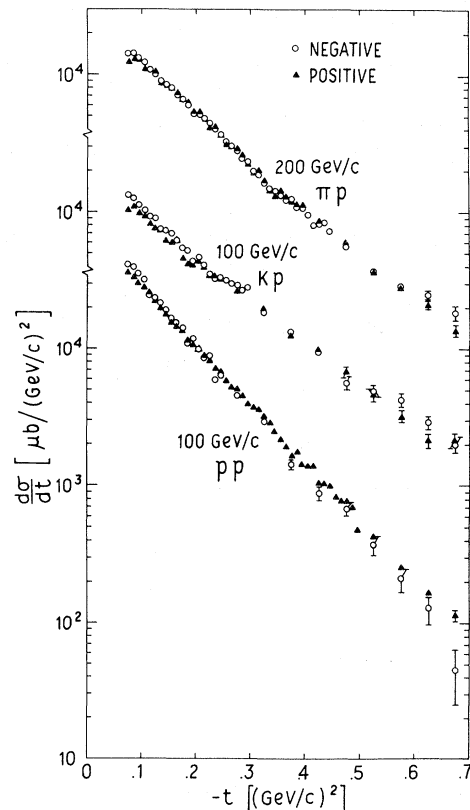


FIG. 7. Comparison of particle and antiparticle elastic scattering.

increasing energy.

A similar comparison can be made for the K^+p and K^-p elastic cross sections; however, both $I=0$ (ω) and $I=1$ (ρ) exchange can occur, with ω exchange dominant. No high-energy measurements exist for the appropriate inelastic channel ($K_L^0 n \rightarrow K_S^0 n$). However, the lower-energy measurements⁹ of $K_L^0 p \rightarrow K_S^0 p$ give the ω trajectory strength. Assuming the same s dependence as for the ρ trajectory, one would predict a larger difference between K^+p and K^-p scattering than between π^+p and π^-p . As shown in Fig. 7 the difference between K^+p and K^-p elastic scattering is small but observable at 100 GeV/c, which is the highest energy at which we have good data on both reactions.

At 100 GeV/c beam momentum the difference in slope between $\bar{p}p$ and pp is also illustrated in Fig. 7. Just as in the case of the meson reactions, this difference is smaller than at lower energies but is still clearly visible.

The energy dependence of the reactions is also important. At lower energies a shrinkage of the width of the forward diffraction peak with increasing energy has been observed for all reactions except $\bar{p}p$, for which the peak expands. This behav-

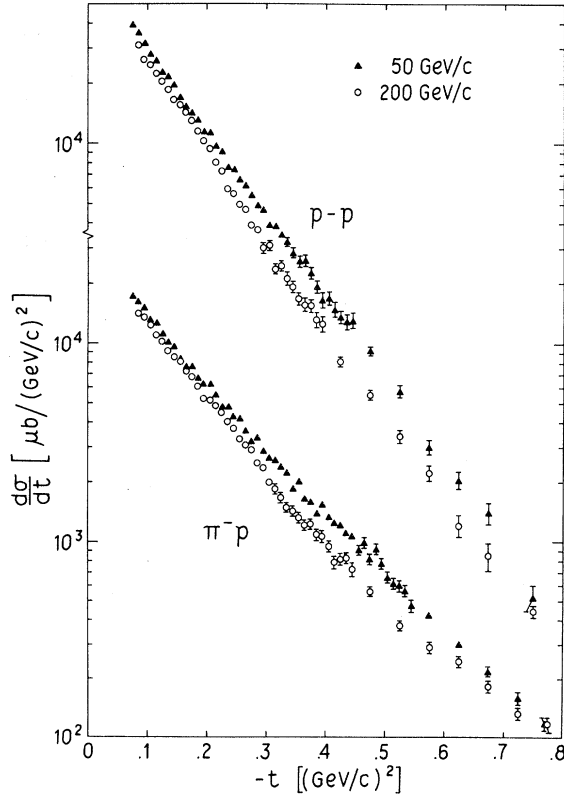


FIG. 8. Energy dependence of pp and π^-p differential elastic cross sections.

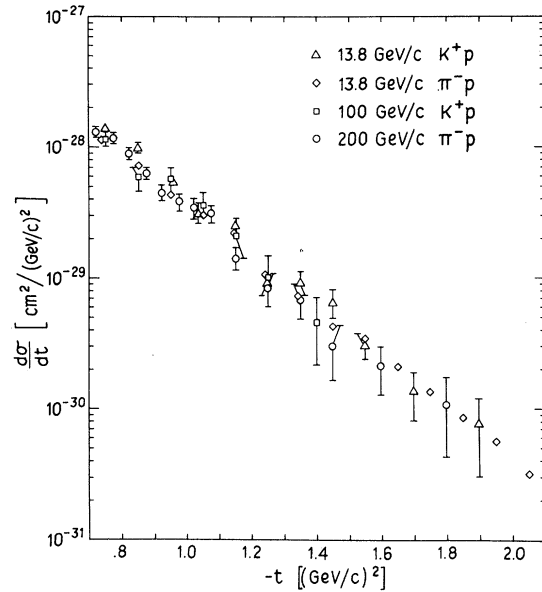


FIG. 9. Behavior at large $-t$ of meson-proton elastic scattering for various energies and particle type. 13.8-GeV/c data are from Rubinstein *et al.*, Ref. 10.

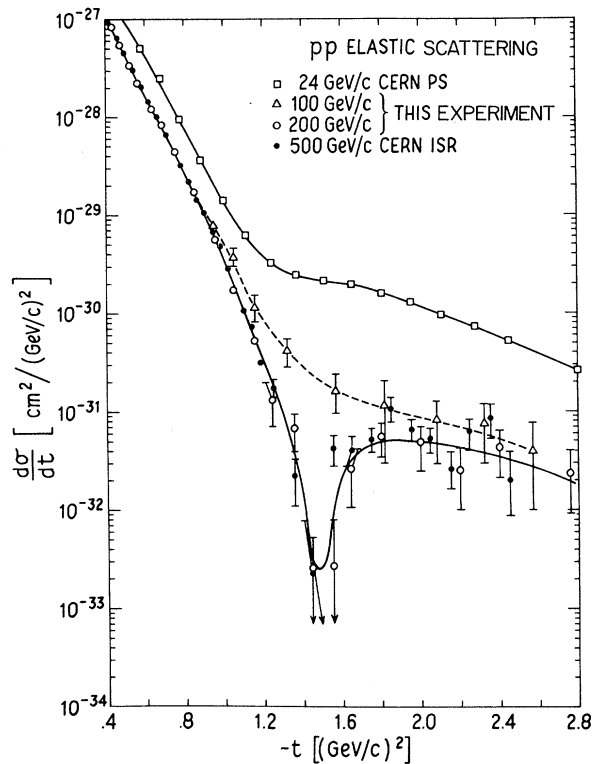


FIG. 10. Energy and t dependence of pp elastic scattering. 24- and 500-GeV/c data are from Ref. 11. The data at 100 GeV/c, because of limited statistical accuracy, do not preclude a moderate dip. The two lowest points at 200 GeV/c are consistent with $d\sigma/dt=0$. The 90% confidence limit is approximately twice the upper error bar.

TABLE I. Data on elastic scattering. Normalization was done by extrapolating a fit of the form e^{bt+ct^2} to the optical point.

$-t$ [(GeV/c) ²]	$d\sigma/dt$ [$\mu\text{b}/(\text{GeV}/c)^2$]	$-t$ [(GeV/c) ²]	$d\sigma/dt$ [$\mu\text{b}/(\text{GeV}/c)^2$]
	π^+p 50 GeV		π^+p 50 GeV
0.075	14 812 \pm 245	0.825	75.9 \pm 7.5
0.085	13 618 \pm 233	0.875	55.1 \pm 6.4
0.095	12 580 \pm 224	0.925	55.1 \pm 6.3
0.105	11 795 \pm 216	0.975	32.9 \pm 4.9
0.115	10 498 \pm 203	1.025	26.0 \pm 4.4
0.125	9780 \pm 196	1.075	17.4 \pm 3.7
0.135	9124 \pm 189	1.125	12.8 \pm 3.1
0.145	8269 \pm 179	1.175	9.5 \pm 2.7
0.155	7562 \pm 171	1.225	14.2 \pm 3.2
0.165	7089 \pm 165	1.300	3.3 \pm 1.2
0.175	6581 \pm 159	1.40	5.4 \pm 1.4
0.185	6248 \pm 155	1.50	1.44 \pm 0.83
0.195	5730 \pm 148	1.65	0.69 \pm 0.43
0.205	5151 \pm 140		
0.215	4958 \pm 137		π^-p 50 GeV
0.225	4570 \pm 133	0.075	15 638 \pm 281
0.235	4106 \pm 126	0.085	14 772 \pm 272
0.245	3604 \pm 121	0.095	13 885 \pm 263
0.255	3524 \pm 116	0.105	12 077 \pm 245
0.265	3430 \pm 115	0.115	11 607 \pm 240
0.275	3081 \pm 109	0.125	10 083 \pm 223
0.285	2792 \pm 103	0.135	9134 \pm 212
0.295	2626 \pm 100	0.145	8789 \pm 207
0.305	2481 \pm 97	0.155	7683 \pm 193
0.315	2295 \pm 93	0.165	6904 \pm 183
0.325	2181 \pm 91	0.175	6941 \pm 184
0.335	1934 \pm 86	0.185	6048 \pm 171
0.345	1788 \pm 82	0.195	5671 \pm 165
0.355	1673 \pm 79	0.205	5758 \pm 166
0.365	1574 \pm 77	0.215	5021 \pm 155
0.375	1442 \pm 74	0.225	4317 \pm 145
0.385	1321 \pm 71	0.235	4352 \pm 145
0.395	1245 \pm 69	0.245	3845 \pm 138
0.405	1161 \pm 66	0.255	3799 \pm 136
0.415	1035 \pm 63	0.265	3235 \pm 125
0.425	956 \pm 60	0.275	2892 \pm 118
0.435	1021 \pm 62	0.285	3079 \pm 122
0.445	891 \pm 58	0.295	2580 \pm 111
0.455	782 \pm 54	0.305	2408 \pm 107
0.465	781 \pm 54	0.315	2362 \pm 106
0.475	721 \pm 52	0.325	2153 \pm 101
0.485	758 \pm 53	0.335	2018 \pm 98
0.495	511 \pm 44	0.345	1658 \pm 89
0.505	633 \pm 48	0.355	1842 \pm 93
0.515	580 \pm 46	0.365	1500 \pm 84
0.525	456 \pm 41	0.375	1433 \pm 82
0.535	484 \pm 42	0.385	1264 \pm 77
0.545	466 \pm 41	0.395	1404 \pm 82
0.555	444 \pm 40	0.405	1185 \pm 75
0.565	355 \pm 36	0.415	1131 \pm 73
0.575	395 \pm 38	0.425	1092 \pm 72
0.585	405 \pm 38	0.435	999 \pm 68
0.595	322 \pm 35	0.445	955 \pm 67
0.625	281 \pm 14	0.455	813 \pm 62
0.675	185 \pm 11	0.465	911 \pm 65
0.725	145 \pm 10	0.475	727 \pm 59
0.775	98.1 \pm 8.5	0.485	844 \pm 63
		0.495	692 \pm 57

TABLE I. (continued)

$-t$ [(GeV/c) ²]	$d\sigma/dt$ [$\mu\text{b}/(\text{GeV}/c)^2$]	$-t$ [(GeV/c) ²]	$d\sigma/dt$ [$\mu\text{b}/(\text{GeV}/c)^2$]
	<i>pp</i> 50 GeV		π^+p 100 GeV
0.875	2.0 ± 4.4	0.295	2261 ± 129
0.925	8.6 ± 5.6	0.305	2003 ± 121
0.975	11.4 ± 5.9	0.315	1677 ± 111
1.025	2.9 ± 3.9	0.325	1851 ± 116
	$\bar{p}p$ 50 GeV	0.335	1607 ± 108
		0.345	1529 ± 105
0.075	50 388 ± 1940	0.355	1545 ± 106
0.085	48 929 ± 1906	0.365	1236 ± 95
0.095	40 576 ± 1731	0.375	1300 ± 97
0.105	32 594 ± 1548	0.385	1263 ± 96
0.115	32 813 ± 1550	0.395	1097 ± 89
0.125	26 687 ± 1394	0.405	1148 ± 91
0.135	23 664 ± 1310	0.415	1054 ± 87
0.145	22 597 ± 1279	0.425	873 ± 79
0.155	21 416 ± 1242	0.435	666 ± 79
0.165	18 202 ± 1144	0.445	726 ± 72
0.175	15 830 ± 1064	0.455	642 ± 68
0.185	14 866 ± 1030	0.465	699 ± 70
0.195	14 406 ± 1013	0.475	565 ± 64
0.205	10 958 ± 883	0.485	583 ± 65
0.215	11 715 ± 912	0.495	439 ± 56
0.225	9579 ± 829	0.525	416 ± 24
0.235	7303 ± 724	0.575	305 ± 21
0.245	9690 ± 831	0.625	254 ± 19
0.275	6046 ± 292	0.675	156 ± 15
0.325	3827 ± 232	0.725	125 ± 13
0.375	1874 ± 162	0.775	94 ± 11
0.425	1083 ± 123	0.825	71 ± 10
0.475	894 ± 111	0.875	56 ± 9
0.525	506 ± 84	0.925	46.8 ± 8.0
0.575	203 ± 54	0.975	25.5 ± 6.5
0.625	244 ± 53	1.025	24.8 ± 5.9
0.675	127 ± 43	1.075	13.5 ± 4.5
0.725	64 ± 31	1.125	8.4 ± 3.6
0.800	2.8 ± 9.0	1.175	8.6 ± 3.6
0.900	24.1 ± 14.3	1.225	6.8 ± 3.2
1.00	24.2 ± 14.0	1.275	6.0 ± 3.0
	π^+p 100 GeV	1.325	5.0 ± 2.7
0.075	14 537 ± 334	1.400	3.14 ± 1.57
0.085	13 630 ± 322	1.50	1.27 ± 1.10
0.095	12 520 ± 308	1.65	0.24 ± 0.6
0.105	11 494 ± 294		
0.115	9649 ± 272	0.075	15 388 ± 314
0.125	9768 ± 270	0.085	15 024 ± 309
0.135	8231 ± 247	0.095	12 925 ± 286
0.145	7623 ± 238	0.105	11 868 ± 273
0.155	6873 ± 225	0.115	10 993 ± 263
0.165	6967 ± 227	0.125	9876 ± 248
0.175	5761 ± 206	0.135	8924 ± 235
0.185	5725 ± 205	0.145	8236 ± 226
0.195	5125 ± 193	0.155	7749 ± 219
0.205	4787 ± 187	0.165	7083 ± 209
0.215	4650 ± 184	0.175	6187 ± 195
0.225	4064 ± 173	0.185	6194 ± 195
0.235	3979 ± 171	0.195	5395 ± 181
0.245	3567 ± 162	0.205	4887 ± 173
0.255	3473 ± 159	0.215	4781 ± 170
0.265	2950 ± 147	0.225	4270 ± 162
0.275	2886 ± 145	0.235	3778 ± 149
0.285	2555 ± 137	0.245	3629 ± 149

TABLE I. (*continued*)

$-t$ [(GeV/c) ²]	$d\sigma/dt$ [$\mu\text{b}/(\text{GeV}/c)^2$]	$-t$ [(GeV/c) ²]	$d\sigma/dt$ [$\mu\text{b}/(\text{GeV}/c)^2$]
	π^+p 100 GeV		K^+p 100 GeV
0.255	3304 \pm 142	0.235	3039 \pm 299
0.265	3207 \pm 140	0.245	2917 \pm 292
0.275	2789 \pm 131	0.275	2381 \pm 117
0.285	2637 \pm 127	0.325	1771 \pm 101
0.295	2390 \pm 121	0.375	1103 \pm 79
0.305	2278 \pm 118	0.425	868 \pm 70
0.315	2052 \pm 112	0.475	617 \pm 59
0.325	2149 \pm 114	0.525	422 \pm 49
0.335	1855 \pm 106	0.575	290 \pm 40
0.345	1696 \pm 101	0.625	195 \pm 33
0.355	1669 \pm 101	0.675	195 \pm 33
0.365	1402 \pm 92	0.725	125 \pm 26
0.375	1391 \pm 91	0.775	90 \pm 22
0.385	1095 \pm 81	0.850	53.9 \pm 12.4
0.395	917 \pm 75	0.950	52.3 \pm 12.0
0.405	921 \pm 75	1.050	33.0 \pm 9.6
0.415	1095 \pm 81	1.150	19.3 \pm 7.3
0.425	934 \pm 75	1.850	9.1 \pm 5.1
0.435	865 \pm 72	1.40	4.2 \pm 2.5
0.445	869 \pm 72		
0.455	866 \pm 72		K^+p 100 GeV
0.465	740 \pm 67	0.075	11 999 \pm 503
0.475	643 \pm 62	0.085	11 390 \pm 488
0.485	623 \pm 61	0.095	9968 \pm 456
0.495	604 \pm 60	0.105	9181 \pm 436
0.525	454 \pm 23	0.115	8300 \pm 414
0.575	335 \pm 20	0.125	8063 \pm 407
0.625	240 \pm 17	0.135	6698 \pm 370
0.675	173 \pm 14	0.145	6583 \pm 367
0.725	107 \pm 11	0.155	6257 \pm 357
0.775	87 \pm 10	0.165	5486 \pm 333
0.825	58 \pm 8	0.175	4903 \pm 314
0.875	58 \pm 8	0.185	4696 \pm 308
0.925	41.4 \pm 7.0	0.195	3886 \pm 279
0.975	24.1 \pm 5.4	0.205	4155 \pm 289
1.05	19.7 \pm 3.4	0.215	3593 \pm 268
1.15	12.2 \pm 2.7	0.225	3119 \pm 253
1.25	6.4 \pm 2.0	0.235	2895 \pm 243
1.35	4.5 \pm 1.7	0.245	2989 \pm 246
1.45	2.5 \pm 1.3	0.255	2824 \pm 239
1.625	0.8 \pm 0.5	0.265	2650 \pm 231
1.825	0.6 \pm 0.4	0.275	2584 \pm 228
	K^+p 100 GeV	0.285	2376 \pm 219
0.075	9708 \pm 544	0.295	2486 \pm 224
0.085	10 406 \pm 561	0.325	1679 \pm 82
0.095	8963 \pm 520	0.375	1160 \pm 68
0.105	8594 \pm 508	0.425	850 \pm 58
0.115	7674 \pm 479	0.475	503 \pm 44
0.125	7014 \pm 456	0.525	438 \pm 41
0.135	6608 \pm 442	0.575	377 \pm 38
0.145	5573 \pm 405	0.625	261 \pm 32
0.155	5474 \pm 401	0.675	181 \pm 26
0.165	5561 \pm 404	0.725	125 \pm 22
0.175	4183 \pm 349	0.775	126 \pm 22
0.185	3879 \pm 336	0.825	85 \pm 18
0.195	3699 \pm 328	0.875	24 \pm 10
0.205	4009 \pm 341	0.950	41 \pm 9
0.215	3585 \pm 322	1.050	28.6 \pm 7.4
0.225	3061 \pm 301	1.150	12.2 \pm 5.0
		1.250	16.7 \pm 5.5

TABLE I. (continued)

$-t$ [(GeV/c) ²]	$d\sigma/dt$ [$\mu\text{b}/(\text{GeV}/c)^2$]	$-t$ [(GeV/c) ²]	$d\sigma/dt$ [$\mu\text{b}/(\text{GeV}/c)^2$]
	<i>K⁺p</i> 100 GeV		<i>pp</i> 100 GeV
1.35	3.1 ± 2.6	1.825	0.11 ± 0.10
1.50	4.02 ± 2.0	2.075	0.077 ± 0.056
1.70	2.86 ± 1.6	2.325	0.075 ± 0.051
	<i>pp</i> 100 GeV	2.575	0.038 ± 0.029
		2.825	0.038 ± 0.029
0.075	34 792 ± 510		<i>p̄p</i> 100 GeV
0.085	31 837 ± 487		
0.095	29 122 ± 464	0.075	37 232 ± 1347
0.105	26 780 ± 444	0.085	35 209 ± 1305
0.115	24 086 ± 420	0.095	31 801 ± 1238
0.125	20 800 ± 390	0.105	28 698 ± 1173
0.135	18 579 ± 367	0.115	22 095 ± 1027
0.145	16 784 ± 349	0.125	21 070 ± 1000
0.155	14 661 ± 325	0.135	19 132 ± 951
0.165	13 575 ± 313	0.145	16 866 ± 892
0.175	12 779 ± 303	0.155	14 807 ± 834
0.185	10 890 ± 279	0.165	13 631 ± 799
0.195	10 178 ± 269	0.175	12 358 ± 760
0.205	9391 ± 258	0.185	9759 ± 674
0.215	8336 ± 245	0.195	10 492 ± 698
0.225	7650 ± 234	0.205	8737 ± 636
0.235	6775 ± 221	0.215	7591 ± 592
0.245	6481 ± 215	0.225	7872 ± 607
0.255	5536 ± 199	0.235	5242 ± 496
0.265	4991 ± 189	0.245	5682 ± 515
0.275	4933 ± 188	0.275	4043 ± 193
0.285	4240 ± 174	0.325	2605 ± 155
0.295	3732 ± 163	0.375	1283 ± 109
0.305	3520 ± 158	0.425	783 ± 87
0.315	3440 ± 156	0.475	610 ± 75
0.325	3078 ± 148	0.525	335 ± 56
0.335	2703 ± 139	0.575	189 ± 43
0.345	2349 ± 129	0.625	115 ± 33
0.355	2084 ± 121	0.675	41 ± 21
0.365	1823 ± 114	0.750	54 ± 16
0.375	1590 ± 106	0.850	9.0 ± 8.4
0.385	1688 ± 109	0.950	4.6 ± 6.4
0.395	1346 ± 98		<i>π⁺p</i> 200 GeV
0.405	1307 ± 96		
0.415	1332 ± 97	0.075	11 212 ± 355
0.425	983 ± 84	0.085	11 536 ± 359
0.435	965 ± 83	0.095	11 537 ± 358
0.445	926 ± 81	0.105	9683 ± 327
0.455	788 ± 75	0.115	9692 ± 327
0.465	732 ± 72	0.125	9254 ± 318
0.475	732 ± 72	0.135	7662 ± 289
0.485	666 ± 69	0.145	7392 ± 283
0.495	450 ± 57	0.155	7100 ± 277
0.525	412 ± 24	0.165	6704 ± 269
0.575	242 ± 17	0.175	6063 ± 255
0.625	159 ± 10	0.185	5510 ± 243
0.675	108 ± 9	0.195	4898 ± 229
0.725	67 ± 8	0.205	4836 ± 227
0.775	42 ± 6	0.215	4127 ± 212
0.825	25 ± 5	0.225	3659 ± 199
0.875	12.8 ± 2	0.235	3698 ± 200
0.95	7.7 ± 0.9	0.245	3210 ± 186
1.050	3.5 ± 0.8	0.255	2690 ± 170
1.150	1.12 ± 0.43	0.265	2617 ± 168
1.325	0.40 ± 0.13	0.275	2471 ± 163
1.575	0.16 ± 0.08	0.285	2304 ± 157

TABLE I. (*continued*)

$-t$ [(GeV/c) ²]	$d\sigma/dt$ [$\mu\text{b}/(\text{GeV}/c)^2$]	$-t$ [(GeV/c) ²]	$d\sigma/dt$ [$\mu\text{b}/(\text{GeV}/c)^2$]
	π^+p 200 GeV		π^-p 200 GeV
0.295	1898 \pm 143	0.345	1279 \pm 85
0.305	1686 \pm 134	0.355	1171 \pm 81
0.315	1751 \pm 137	0.365	1072 \pm 78
0.325	1467 \pm 125	0.375	1090 \pm 78
0.335	1289 \pm 117	0.385	957 \pm 74
0.345	1154 \pm 111	0.395	950 \pm 74
0.355	1270 \pm 116	0.405	841 \pm 69
0.365	1204 \pm 113	0.415	695 \pm 63
0.375	1028 \pm 105	0.425	721 \pm 64
0.385	993 \pm 103	0.435	737 \pm 64
0.395	1006 \pm 104	0.445	642 \pm 60
0.425	761 \pm 40	0.475	491 \pm 23
0.475	544 \pm 33	0.525	328 \pm 19
0.525	334 \pm 26	0.575	254 \pm 17
0.575	241 \pm 22	0.625	217 \pm 15
0.625	182 \pm 20	0.675	163 \pm 13
0.675	119 \pm 16	0.725	117 \pm 11
0.725	109 \pm 15	0.775	104 \pm 11
0.775	87 \pm 14	0.825	79 \pm 9
0.825	70 \pm 12	0.875	55.8 \pm 8
0.875	46.9 \pm 10.0	0.925	39.3 \pm 7
0.925	23.9 \pm 7.5	0.975	34.0 \pm 6.3
0.975	27.0 \pm 7.9	1.025	30.8 \pm 6.0
1.025	13.7 \pm 6.0	1.075	28.0 \pm 5.8
1.075	6.2 \pm 4.7	1.15	12.7 \pm 2.8
1.125	14.4 \pm 5.7	1.25	7.50 \pm 2.40
1.20	9.5 \pm 3.4	1.35	6.08 \pm 2.00
1.30	6.0 \pm 2.8	1.45	2.68 \pm 1.40
1.40	6.3 \pm 2.7	1.55	2.21 \pm 1.30
1.55	0.94 \pm 1.03	1.65	1.58 \pm 1.20
1.75	0.29 \pm 0.77	1.75	1.11 \pm 1.00
	π^-p 200 GeV	1.85	0.82 \pm 0.90
		2.025	0.52 \pm 0.48
		2.375	0.13 \pm 0.19
0.075	12774 \pm 276		K^+p 200 GeV
0.085	12762 \pm 275		
0.095	12005 \pm 266		
0.105	11038 \pm 255	0.075	9970 \pm 878
0.115	9739 \pm 239	0.085	8219 \pm 794
0.125	9006 \pm 229	0.095	8954 \pm 827
0.135	8117 \pm 217	0.125	6706 \pm 316
0.145	7599 \pm 210	0.175	5149 \pm 275
0.155	7174 \pm 203	0.225	3794 \pm 237
0.165	6418 \pm 192	0.275	2088 \pm 175
0.175	6019 \pm 185	0.325	1407 \pm 143
0.185	5379 \pm 175	0.375	1016 \pm 122
0.195	4689 \pm 163	0.425	773 \pm 106
0.205	4620 \pm 162	0.475	550 \pm 89
0.215	4338 \pm 157	0.525	400 \pm 76
0.225	3988 \pm 150	0.575	191 \pm 53
0.235	3573 \pm 142	0.625	258 \pm 61
0.245	3304 \pm 136	0.675	121 \pm 43
0.255	2937 \pm 128	0.725	134 \pm 44
0.265	2729 \pm 124	0.775	55 \pm 29
0.275	2576 \pm 120	0.825	89 \pm 36
0.285	2217 \pm 111	0.875	69 \pm 32
0.295	2104 \pm 108	0.925	92 \pm 36
0.305	1779 \pm 101	0.975	27 \pm 20
0.315	1647 \pm 97	1.050	21.2 \pm 13.2
0.325	1484 \pm 92	1.200	10.4 \pm 7.2
0.335	1321 \pm 86	1.40	3.7 \pm 4.0

TABLE I. (continued)

$-t$ [(GeV/c) ²]	$d\sigma/dt$ [$\mu\text{b}/(\text{GeV}/c)^2$]	$-t$ [(GeV/c) ²]	$d\sigma/dt$ [$\mu\text{b}/(\text{GeV}/c)^2$]
	K^-p 200 GeV		pp 200 GeV
0.075	11 227 ± 1256	0.335	2030 ± 145
0.085	10 822 ± 1229	0.345	1828 ± 138
0.095	10 882 ± 1229	0.355	1598 ± 129
0.125	7411 ± 447	0.365	1499 ± 125
0.175	5791 ± 393	0.375	1470 ± 124
0.225	3724 ± 316	0.385	1251 ± 115
0.275	2435 ± 255	0.395	1198 ± 112
0.325	1693 ± 212	0.425	771 ± 40
0.375	1015 ± 164	0.475	522 ± 33
0.425	830 ± 148	0.525	321 ± 26
0.475	631 ± 128	0.575	210 ± 21
0.525	316 ± 91	0.625	113 ± 16
0.575	218 ± 76	0.675	80 ± 14
0.65	196 ± 51	0.75	42 ± 3
0.75	149 ± 44	0.85	18 ± 2
0.85	65 ± 30	0.95	5.4 ± 0.6
1.00	36 ± 15	1.05	1.7 ± 0.3
		1.150	0.48 ± 0.17
		1.25	0.12 ± 0.07
	pp 200 GeV		
0.075	30 227 ± 573	1.35	0.065 ± 0.029
0.085	29 510 ± 564	1.45	0.0025 ± 0.0052
0.095	24 883 ± 519	1.55	0.0027 ± 0.0052
0.105	23 595 ± 503	1.65	0.026 ± 0.019
0.115	21 311 ± 477	1.80	0.052 ± 0.021
0.125	19 404 ± 454	2.00	0.046 ± 0.022
0.135	17 610 ± 431	2.20	0.025 ± 0.016
0.145	15 830 ± 408	2.40	0.040 ± 0.021
0.155	14 882 ± 395	2.75	0.024 ± 0.016
0.165	13 699 ± 379	3.25	0.012 ± 0.013
0.175	12 365 ± 359		
0.185	11 040 ± 339		
0.195	9800 ± 319		
0.205	8960 ± 304		
0.215	7677 ± 284	0.075	40 471 ± 5181
0.225	7009 ± 271	0.085	28 992 ± 4370
0.235	5663 ± 244	0.095	28 860 ± 4350
0.245	5385 ± 237	0.125	19 785 ± 1589
0.255	4757 ± 223	0.175	13 485 ± 1303
0.265	4494 ± 217	0.225	5989 ± 874
0.275	3719 ± 197	0.275	3863 ± 700
0.285	3538 ± 192	0.325	2006 ± 505
0.295	2887 ± 174	0.375	1031 ± 364
0.305	2968 ± 176	0.425	548 ± 269
0.315	2264 ± 154	0.500	257 ± 132
0.325	2336 ± 156	0.600	85 ± 82
		0.750	8 ± 28
			$\bar{p}p$ 200 GeV final data

ior continues at higher energy as illustrated in Fig. 8. It will be discussed quantitatively later.

An interesting feature of the reactions that can be seen from Fig. 8 is that the shrinkage does not persist to large $-t$ values. In fact beyond $-t=0.8$ (GeV/c)² the meson cross sections are independent of both energy¹⁰ and meson type as seen in Fig. 9. This striking and rather unexpected regularity deserves further study with higher statistics.

For pp elastic scattering at $-t > 1$ (GeV/c)² data

from CERN have shown considerable structure.¹¹ At laboratory momenta of 30 GeV/c the structure takes the form of a sharp break from an exponential; the cross section is considerably flatter at $-t > 1.3$ (GeV/c)² than at smaller t values. At ISR energies (beyond 270 GeV/c equivalent lab momentum) this break has been replaced by a sharp dip at $-t \sim 1.4$ (GeV/c)². The dip is usually attributed to the first minimum in the diffraction pattern and its absence at lower energies is thought

to be connected with a filling in by a real part of the amplitude. As seen in Fig. 10 our data indicate that the dip structure becomes prominent between 100 and 200 GeV/c.

The data are presented in Table I. Because the absolute normalization is uncertain by $\pm 7\%$, the data were normalized to the optical point to facilitate comparison between different types of mesons. The procedure adopted was that of fitting the data to the form e^{bt+ct^2} and extrapolating the curve to $-t=0$. This method is useful for comparison and is more accurate than the absolute normalizations for meson-proton reactions. The normalization to the optical point was consistent with absolute normalization within the errors. No additional correction was made for the known break in the pp cross section around $-t=0.1$ (GeV/c)².

The results of a fit to the data of the form e^{bt+ct^2} are given in Table II. The χ^2 values for the fits are satisfactory except for πp and pp at 200 GeV/c, where the curvature near $-t=0.4$ (GeV/c)² is too great to allow a simultaneous fit of the entire t region with reasonable χ^2 . The data have also been fitted by the sum of two exponentials, which fits all of the data with reasonable χ^2 . The slopes for the various reactions as a function of s evaluated from the e^{bt+ct^2} fit at $-t=0.2$ (GeV/c)² are shown in Fig. 11.

A comparison shows that our fits to the form e^{bt+ct^2} and those of Ref. 4 are generally not in great disagreement. Where occasional disagreements occur, they can be traced back to differences between the t regions being fitted rather than to substantive differences in the data. The data in Ref. 4 extend to slightly smaller $-t$ values than ours but not to such high $-t$ values.

We have examined the problem of determining the crossover point of the particle and antiparticle cross sections, but the cross sections are so close

together that any method which has been considered is hazardous.

In the case of π^*p there is no statistically significant difference between particle and antiparticle data at any t value. For K^*p the particle and antiparticle cross sections differ significantly for $-t < 0.15$ (GeV/c). However, at larger $-t$ no statistically significant differences exist. For pp and $\bar{p}p$ the data differ enough in slope so that in principle a crossover point could be determined, but the normalization uncertainties are too great to allow us to reach any conclusion. A useful measurement of the crossover points will require relative normalizations reliable to 1% or better.

Another quantity of some interest is the ratio of elastic to total cross section. This ratio is shown in Table III, where the normalization using the e^{bt+ct^2} fit was used. An interesting observation is that all the meson-proton elasticities are similar in size and differ by a factor of $\frac{2}{3}$ from the baryon-proton elasticities.

CONCLUSIONS

The extension of elastic-scattering measurements into the region above 50 GeV/c has added measurably to our picture of the Pomeron. At $-t < 0.4$ (GeV/c)² the diffraction peaks shrink with increasing energy (except for $\bar{p}p$).

At $-t > 0.8$ (GeV/c)² the behavior of the meson-proton elastic scattering is independent of both energy and meson type. In an impact-parameter picture it is as if reactions were developing a larger and larger halo as s increases but the behavior for small-impact-parameter collisions remains unchanged. This core region of the interaction behaves independently of whether K or π mesons are used as projectiles despite considerable difference between Kp and πp scattering at

TABLE II. Slope parameters for a fit to the form e^{bt+ct^2} . b is in (GeV/c)⁻², c in (GeV/c)⁻⁴.

	50 GeV/c		100 GeV/c		200 GeV/c	
	b	c	b	c	b	c
π^*p	8.29 ± 0.07	1.37 ± 0.08	8.85 ± 0.09	1.72 ± 0.09	9.25 ± 0.12	1.97 ± 0.14
πp	8.60 ± 0.07	1.71 ± 0.08	8.94 ± 0.08	1.79 ± 0.08	9.26 ± 0.06	2.00 ± 0.05
K^*p	7.30 ± 0.45	1.11 ± 0.53	8.02 ± 0.21	1.60 ± 0.23	8.13 ± 0.37	1.47 ± 0.48
$K p$	7.83 ± 0.37	1.43 ± 0.44	8.53 ± 0.15	1.90 ± 0.15	8.79 ± 0.53	2.21 ± 0.72
pp	9.79 ± 0.15	0.45 ± 0.24	10.42 ± 0.09	0.85 ± 0.13	10.73 ± 0.12	0.82 ± 0.17
$\bar{p}p$			11.87 ± 0.30	1.85 ± 0.52		

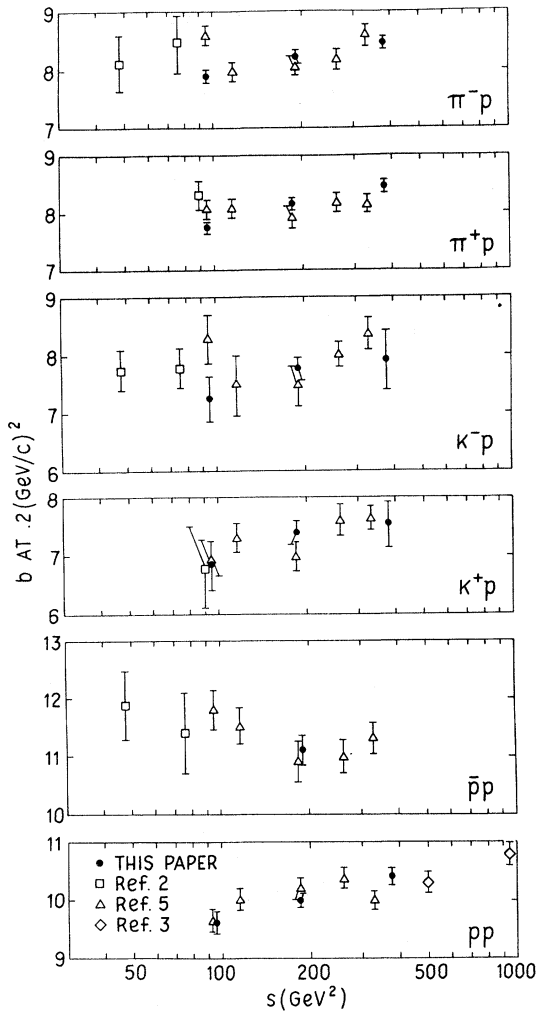


FIG. 11. Slope parameters at $-t=0.2$ $(\text{GeV}/c)^2$ as a function of s . In addition to our data results are shown from Refs. 2, 3, and 4. b is in $(\text{GeV}/c)^{-2}$.

TABLE III. Ratio of elastic to total cross section.

	50 GeV/c	100 GeV/c	200 GeV/c
π^+p	0.144 ± 0.012	0.135 ± 0.012	0.130 ± 0.012
π^-p	0.142 ± 0.012	0.135 ± 0.012	0.129 ± 0.012
K^+p	0.130 ± 0.012	0.123 ± 0.012	0.129 ± 0.012
K^-p	0.135 ± 0.012	0.125 ± 0.012	0.126 ± 0.012
$\bar{p}p$	0.203 ± 0.015	0.188 ± 0.015	0.183 ± 0.015
pp	0.207 ± 0.015	0.177 ± 0.015	0.193 ± 0.015

small $-t$.

The problem of measuring the crossover points has become extremely difficult in the Fermilab energy range because the particle and antiparticle cross sections are so similar. A reliable experiment to measure crossover points would require extremely accurate relative normalizations and should probably include data in the very-small- t region so that an extrapolation to the optical point could be done as a check.

This experiment has also established that the $-t=1.4$ $(\text{GeV}/c)^2$ dip in pp elastic scattering becomes prominent between 100 and 200 GeV/c laboratory momentum. Clearly more data at more energies would be desirable in this t region to elucidate the details of the dip.

ACKNOWLEDGMENT

We would like to thank the Fermilab Accelerator and Meson Lab staffs. Also, we would like to thank R. Thun, J. Koschik, and M. Zumberge for valuable assistance during the experiment and P. Kraushaar for help with the analysis.

*Work supported by the U.S. Energy Research and Development Administration.

†Present address: Max-Planck-Institut für Physik and Astrophysik, München, West Germany.

‡Present address: Fermi National Accelerator Laboratory, Batavia, Illinois 60510.

§Present address: Stanford Linear Accelerator Center, Stanford, California 94720.

¹T. Lasinski *et al.*, Nucl. Phys. B37, 1 (1972).

²Y. Antipov *et al.*, Nucl. Phys. B57, 333 (1973); in *Proceedings of the XVII International Conference on High Energy Physics, London, 1974*, edited by J. R. Smith (Rutherford Laboratory, Chilton, Didcot, Berkshire, England, 1974), p. I-25; A. Derevchikov *et al.*, Phys. Lett. 48B, 367 (1974).

³G. Barbiellini *et al.*, Phys. Lett. 39B, 663 (1972); M. Holder *et al.*, *ibid.* 35B, 355 (1971); M. Holder

et al., *ibid.* 36B, 400 (1971).

⁴Fermilab Single Arm Spectrometer Group, Phys. Rev. Lett. 35, 1195 (1975).

⁵C. Akerlof *et al.*, Phys. Lett. 59B, 197 (1975); C.

Akerlof *et al.*, Phys. Rev. Lett. 35, 1406 (1975).

⁶W. F. Baker *et al.*, Phys. Lett. 51B, 303 (1974).

⁷S. Pruss, Fermilab Report No. P.N. 298 (unpublished).

⁸A. V. Barnes *et al.*, in *Proceedings of the XVII International Conference on High Energy Physics, London, 1974*, edited by J. R. Smith (Rutherford Laboratory, Chilton, Didcot, Berkshire, England, 1974), p. I-37; private communication.

⁹G. W. Brandenburg *et al.*, Phys. Rev. D 9, 1939 (1974).

¹⁰R. Rubinstein *et al.*, Phys. Rev. Lett. 30, 1010 (1973).

¹¹J. Allaby *et al.*, Nucl. Phys. 52B, 316 (1973); A. Böhm *et al.*, Phys. Lett. 49B, 491 (1974).